VOLUME 8, NUMBER 5, MAY 2008

NANO LETTERS

Catalytic Motors for Transport of Colloidal Cargo

Shakuntala Sundararajan,[†] Paul E. Lammert,[‡] Andrew W. Zudans,[†] Vincent H. Crespi,*[,‡] and Ayusman Sen*[,†]

Departments of Chemistry and Physics, The Pennsylvania State University, University Park, Pennsylvania 16802

Received September 6, 2007; Revised Manuscript Received March 18, 2008

ABSTRACT

Autonomous micro- and nanomotors should, in principle, deliver materials in a site-directed fashion, powering the assembly of dynamic, nonequilibrium superstructures. Here we demonstrate that catalytic Pt−Au nanomotors can transport a prototypical cargo: polystyrene microspheres. In addition, motors with Ni segments can overcome both Brownian orientational fluctuations and biased rotation of the rod−sphere doublet to enable persistent steerable uniaxial motion in an external magnetic field. Assuming a cargo-independent motive force, the speeds are inversely proportional to the Stokes resistance, which we compute using a completed double-layer boundary integral equation. In addition, we demonstrate motors transporting cargo via chemotaxis toward a H_2O_2 fuel source.

The design and application of micro- and nanoscale motors propelled by self-generated forces has sustained substantial interest in the scientific community in recent years. While our ability to synthesize materials in varied geometries with unique properties is well-established, our capacity to precisely control the placement and transport of objects at this size scale is much more limited. Low-frequency external electric and magnetic fields can sort and separate ensembles of colloids, while high-frequency electromagnetic fields in optical tweezers can maneuver individual colloids with nanometer-scale precision.[1–3] Neither technique enables independent autonomous directed motion of each object in an ensemble. Such a level of control is possible only if each object can actively interact with its surroundings to propel itself. Such miniature workhorses could then be programmed to control the transport and organization of materials at the mesoscopic level, as inspired by the elegant chemomechanical ballet that is cellular biology. Such capabilities would be valuable for bottom-up assembly of superstructures and devices, targeted delivery of chemicals, roving sensors, etc.

Several research groups have harvested biomotors and reported their ability to carry loads in vitro.[4] However, replicating their sophisticated motor function outside biology is a daunting challenge, due to their inherent complexity. Moreover, the lifetime of such devices is limited because biomotors, being tied to the precisely tuned physiology of the cell, degrade rapidly outside of the cellular support system. Simply scaling down macroscale motors is not viable due to limitations in fabricating complex architectures at the mesoscale and the profound differences between the familiar

* Corresponding author. E-mail: asen@psu.edu. Telephone: 814-863-2460. Fax: 814-865-1543.
† Department of Chemistry.
‡ Department of Physics.

10.1021/nl072275j CCC: $40.75
Published on Web 04/17/2008

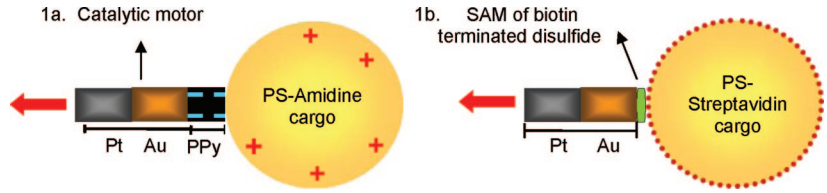

Figure 1. Cargo attachment by (a) electrostatic interaction between the negative PPy end of a Pt−Au−PPy motor and a positively charged PS amidine microsphere and (b) biotin−streptavidin binding between the Au tips of Pt−Au rods functionalized with a biotin-terminated disulfide and streptavidin-coated cargo.

macroscale regime and highly overdamped aqueous mesoscopia.[5]

We and others have designed motors powered via the asymmetric placement of onboard catalyst.[6] For example, our group has previously reported the motility of micrometer sized Pt−Au rods in aqueous hydrogen peroxide solutions via self-electrophoresis. The object creates its own electric field via bipolar decomposition of hydrogen peroxide.[7,8] Bimetallic rods of other metals such as Ni−Au, Rh−Au, etc., also move in accord with a self-electrophoretic mechanism.[9] This phenomenon has also been used to make micropumps.[10] Here we present the first quantitative study of a nonbiological nanomotor's cargo-carrying capability, elucidating systematic trends in motor speed as a function of cargo radius and demonstrating that magnetic steering elements can overcome the enhanced rotational diffusion of a large spherical cargo (and the biased rotation of an asymmetric rod-sphere doublet) to enable persistent directed motion. While the drag on regular shapes like spheres and cylinders is well-known, the shape of the motor−cargo doublet is unique. We have computed the drag on the rod−sphere doublets using a boundary integral equation and thereby demonstrate that doublets with largest-radius cargos exhibit an anomalously large motility.

Attaching Colloidal Cargo to Catalytic Nanomotors. Pt−Au rods were prepared by galvanostatic deposition in the pores of alumina membranes and released as described previously.[11] Briefly, a sacrificial silver layer was deposited to block the branched portion of the membrane, followed by platinum and finally gold deposition. Pt−Au−PPy and Pt−Ni−Au−Ni−Au−PPy rods were prepared in a similar fashion, with the PPy being deposited last.[12] The electropolymerization of the aqueous 0.5 M pyrrole solution was carried out in the presence of 0.1 M KCl by cycling the potential between 0.8 and 1.0 V vs Ag/AgCl at 20 mV/s.[13] All electrodeposition steps were carried out using a potentiostat (Pine model AFRED5). The lengths of the Pt and Au segments were approximately 1.2 μm each in Pt−Au and Pt−Au−PPy rods. In Pt−Ni−Au−Ni−Au−PPy rods the Pt segment was nearly 1.2 μm, the Ni segments were 100 nm long and separated by a 200 nm long gold segment, while the terminal Au segment was nearly 800 nm long. The length of the polypyrrole segment ranged from 100 to 800 nm. The diameter of the rods is approximately 370 nm. Lengths were characterized by transmission electron microscopy (JEOL 1200 EXII), scanning electron microscopy (JEOL JSM 5400), and dark-field optical microscopy (Zeiss Axiovert 200 reflectance/transmission).

Pt−Au, Pt−Au−PPy, and Pt−Ni−Au−Ni−Au−PPy motors were attached to polystyrene cargo of varying radii. To provide a reasonably consistent geometry, we attach the cargo always to the tip of the rod, using the two methods shown in Figure 1. First, electrostatic interaction was used to attach positively charged polystyrene−amidine microspheres (Interfacial Dynamics) to a negatively charged PPy segment at one end of the rods. The polypyrrole segment enabled preferential attachment of the cargo, as it bears a more negative zeta potential (−35 mV) than the metal segment (−10 mV), as determined by zeta potential measurements (Brookhaven Zeta PALS) of PPy rods and Pt−Au rods. A 1:2 mixture of rods and spheres was allowed to couple over several minutes. Subsequently, the autonomous motion of the motor-cargo doublets in aqueous 5% H_2O_2 solution was observed through an optical microscope. The great majority of doublets had the sphere fixed to the desired PPy/gold end; a few motors pushed rather than pulled their cargos, which were nonspecifically bound to the Pt end.

The second attachment method used a more specific biotin−streptavidin interaction. The Au ends of the Pt−Au rods in-membrane (with no PPy segment) were exposed to an 1 mM ethanolic solution of biotin-terminated disulfide; EZ-Link Biotin HPDP (Pierce)[14] to form a self-assembled monolayer of biotin-terminated disulfide. The functionalized rods were released by dissolving the membrane in dilute NaOH and subsequently mixed with streptavidin-coated microspheres (Polysciences). While the latter method gave higher yields of doublets with the desired geometry, the former method was used for further quantitative study of rod motion because positively charged amidine-coated microspheres are available in a wider range of radii than streptavidin-coated microspheres.

Effect of Cargo Attachment. We attached amidine-functionalized PS microsphere cargo of radii 0.38, 0.60, 1.05, and 1.65 μm. Figure 2 shows a Pt−Au−PPy motor in action linked to a 1.05 μm cargo. Video clips were recorded using an optical microscope equipped with a digital video camera connected to a PC. A video clip of a motor attached to 1.05 μm radius cargo is available as Supporting Information. A steady decrease in speed with increasing cargo radius was anticipated. The 1.65 μm spheres slowed rods to such an extent that translational motion was barely discernible, although non-Brownian rotational motion could be observed in some doublets. Table 1 shows the doublet speed as a function of cargo radius (these are discussed in greater detail below). Columns I, II, and III are repetitions with different batches of rods. Each entry is an average over 20 or more

Figure 2. Transmission optical microscopy images of a Pt−Au−PPy motor pulling 1.05 μm radius cargo, showing the trajectory over 4 s. Images were captured at 1000× magnification.

Table 1. Effect of Cargo Radii on Pt−Au−PPy Motor Speed[a]

	speed (μm/s)		
cargo radius (μm)	I	II	III
0	7.4 ± 0.3	6.4 ± 0.2	6.1 ± 0.1
0.38	5.9 ± 0.4	5.1 ± 0.1	4.7 ± 0.3
0.6	4.9 ± 0.2	4.3 ± 0.1	3.7 ± 0.3
1.05	3.9 ± 0.2	3.5 ± 0.1	3.0 ± 0.1

[a] Columns I, II, and III are repetitions of the experiment with different sets of rods. Each entry is the average of over 20 or more rods, and the sample standard deviations are indicated alongside.

rods; the sample standard deviations are indicated alongside. To determine doublet velocities, videos clips were analyzed by an internally developed MATLAB-based particle tracking program. All trajectory data, for both diffusive and powered motion, were collected within 5 min of placing the solution on a glass slide.

Pt−Au rods and rod−sphere doublets typically sit 2−3 μm above the surface of the glass. Does the interaction between the positively charged microspheres and the oppositely charged glass substrate affect the doublet speed? Any impediment due to this interaction would be revealed by a lowering of the diffusion coefficient below that expected for a free particle in two dimensions. We therefore measured the translational diffusion coefficients in water of the 0.6, 1.05, and 1.65 μm radius spheres (without motors) when sitting 2−3 μm above the surface. The measured average diffusion coefficients of particles after 5 min for 0.6, 1.05, and 1.65 μm radius spheres are 4.3×10^{-13}, 2.2×10^{-13}, and 0.8×10^{-13} m^2/s, respectively, compared to theoretical values of 4.1×10^{-13}, 2.0×10^{-13}, and 1.9×10^{-13} m^2/s. The close agreement between the theory and experiment for the 0.6 and 1.05 μm spheres suggests that the interaction between these spheres and the glass substrate is minimal. The lower experimental diffusion coefficient for the largest (1.65 μm) spheres indicates that substrate effects cannot be neglected in this case: at this separation from the surface a 1.65 μm radius cargo is nearly dragging on the surface, and rods attached to such spheres are greatly hindered. The diffusion coefficients in water of doublets with 0.6 and 1.05 μm spheres were also measured; they are reasonably stable over the course of 30 min (see Supporting Information). Doublets have smaller diffusion coefficients than the plain spheres, as expected. Since all videos of non-Brownian motion are recorded within the first 5 min of placing the solution over the glass slide, the stability of both sphere and doublet diffusion over much longer times suggests that substrate−cargo interaction has a negligible effect on doublet speed for 0.6 and 1.05 μm radius cargo.

Remote-Controlled Pt−Ni−Au−Ni−Au-PPy Motors for Increased Directionality. Unconstrained autonomously moving catalytic motors, with or without cargo, exhibit orientational diffusion. In addition, rods which are attached asymmetrically to cargo tend to exhibit a sustained biased rotation, an effect that is more pronounced at larger cargo diameters. For applications such as transport and delivery in the mesoscale, it is necessary to overcome these two effects and sustain directionality across both time and space.

Hence we have incorporated thin Ni segments into the motors, with the overall segment sequence Pt−Ni−Au−Ni−Au−PPy.[12] Such motors can be oriented by an external magnetic field because the Ni segments experience a magnetic torque. Two small NdFeB bar magnets, parallel and equidistant from the sample on opposite sides, produce a field of a few hundred gauss. The external magnetic field completely suppresses the orientational drift and diffusion, except for a residual fluctuation about the preferred axis (perpendicular to the field direction and parallel to the surface of the slide), as shown in Figure 3. Video clips of a motor attached to 0.6 μm radius cargo in the presence and absence of the external magnetic field are available as Supporting Information.

Table 2 summarizes the rotational characteristics of ~10 doublets for each cargo size (radii: 0.38, 0.60, and 1.05 μm), as well as rods with no cargo, in the absence and presence of the magnetic field. Motions with or without magnetic field are qualitatively distinct, so different physical quantities (with different units) are necessary to describe them. Motion without field is characterized by a biased rotational drift (measured in degrees per second) superimposed with an orientational diffusion (measured by a diffusion constant in degrees^2 per second). Motion with field involves neither drift nor diffusion but simply a characteristic magnitude for angular fluctuations about the mean orientation. With no field, orientational drift of tens of degrees per second and effective rotational diffusion coefficients D_{rot} of several hundred to a few thousand degrees squared per second are common. Such values of D_{rot} are consistent with a purely thermal origin of the orientational diffusion, but there may be a significant component related to fluctuations in the reaction distribution and flexing of the PPy linkers. Doublets with 1.05 μm cargo have much slower rotational motion, as is to be expected. When the external field is imposed, the ability of rotationally biased doublets to cycle through 360° is fully quenched. The doublets are well-oriented, exhibiting fluctuations of only a few degrees, as shown in the table. While small, these orientational fluctuations are an order of magnitude larger than thermal fluctuations would produce if the net magnetic moments of the two Ni segments were

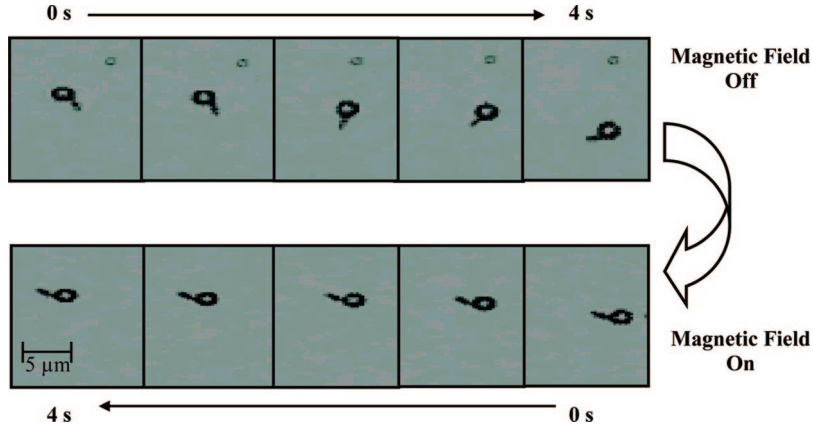

Figure 3. Transmission optical microscopy images of a Pt−Ni−Au−Ni−Au-PPy motor pulling 1.05 μm radius cargo, showing the trajectory over 4 s. Images were captured at 1000× magnification. The top pane shows the trajectory in the absence of the field while the bottom pane shows the trajectory in the presence of the field. The external magnetic field suppresses the rotation of the doublet.

Table 2. Effect of External Magnetic Field on Pt−Ni−Au−Ni−Au-PPy Motors with Cargo of Various Radii[a]

	rods		0.38 μm cargo		
particle no.	D_{rot} (deg^2/s)[field off]	wobble (deg)[field on]	drift (deg/s)[field off]	D_{rot} (deg^2/s)[field off]	wobble (deg)[field on]
1	1072	4.8	−104 ± 26	3207	7.3
2	666	9.6	−173 ± 33	5058	6.7
3	3602	7.7	−174 ± 18	1476	5.1
4	1317	3.7	−193 ± 54	13444	6.9
5	2540	6.0	−44 ± 22	2349	5.0
6	2809	8.5	−6 ± 22	2353	8.7
7	562	7.6	−61 ± 20	1943	6.1
8	1790	5.7	73 ± 14	979	6.1
9	834	3.3	−73 ± 18	1498	5.9
10	573	5.9	−9 ± 27	3334	8.7

	0.60 μm cargo			1.05 μm cargo		
particle no.	drift (deg/s) [field off]	D_{rot} (deg^2/s) [field off]	wobble (deg) [field on]	drift (deg/s) [field off]	D_{rot} (deg^2/s) [field off]	wobble (deg) [field on]
1	1 ± 12	617	8.7	0 ± 9	403	3.8
2	16 ± 12	664	5.4	0.0 ± 6	149.7	4
3	−16 ± 13	816	3.1	11 ± 6	174.9	3.9
4	20 ± 14	933	7.7	11 ± 8	295	3.8
5	−22 ± 12	620	3.7	14 ± 8	280	7
6	−42 ± 8	282	5.6	16 ± 10	464	4.8
7	33 ± 16	1243	5.8	18 ± 8	292	5.4
8	35 ± 12	674	3.9	−20 ± 6	172	5.6
9	−42 ± 13	768	7.3	37 ± 6	166	3.2
10	−5 ± 12	672	5.4	5.7 ± 8	328.4	6.2

[a] For each doublet or unloaded motor, five second video clips were taken in the absence and presence of a few hundred gauss field from a handheld magnet. In absence of a field, the orientational motion is assumed to consist of a steady rotational drift velocity (biased rotation) with rotational diffusion superimposed. The steady drift and rotational diffusion coefficient (D_{rot}) are extracted from a statistical analysis. There is a large uncertainty in the drifts due to the short length of the video clips. With the field on, the motors are strongly oriented along a direction perpendicular to the magnetic field. The reported wobble (with the field on) is the standard deviation of the orientation—in this case, the drift and diffusion coefficients are effectively zero over long times.

aligned and saturated. This is not surprising, since the "two Ni pancake" geometry is designed such that the fields which the two segments exert on each other are comparable to or greater than the external field, and these self-fields favor opposite moments. More highly magnetized rods are not currently useful since they agglomerate so strongly as to interfere with doublet formation.

Chemotaxis of Motor Cargo Doublets. Magnetic steering provides one means of directional control, but standard laboratory fields are essentially uniform across the sample; such fields can impose only divergence-free director field constraints on cargo motion. More precise control, e.g., delivery to a specific point in space, requires motive constraints that pick one point in space as special. To this end, we exploit the recently discovered phenomenon of motor chemotaxis to deliver cargo to specific local maxima in H_2O_2 concentration.[15] We placed a mixture of Pt−Au−PPy rods and 0.6 μm radius spheres in a H_2O_2 gradient generated by placing a piece of agar gel soaked in 30% H_2O_2 in the center of a glass slide. A gasket was placed on the glass slide and filled with a motor−cargo mixture. The video clip in the Supporting Information section demonstrates the resulting chemotaxis of three doublets toward the gel. The video clip was recorded within 10 min of establishing the concentration gradient and captured at 500× magnification.

Calculation of Drag on the Rod−Cargo Doublets. In our current understanding, electrochemical activity generates a persistent electric field which drives ion currents in the

Table 3. Experimentally Observed Doublet Speeds vs Theoretical Expectations Based on Completed Double-Layer Boundary-Integral Equation (CDL-BIEM) Calculations[a]

			experimentally observed velocity ratio ($U_{doublet}/U_{rod}$)		
R_{cargo} (μm)	R_{eq} doublet calculated by CDL-BIEM (μm)	velocity ratio predicted by R_{eq}	I	II	III
0	0.46−0.53	NA	NA	NA	NA
0.38	0.59−0.65	0.78−0.81	0.80 ± 0.03	0.79 ± 0.01	0.76 ± 0.04
0.6	0.76−0.81	0.61−0.66	0.67 ± 0.01	0.67 ± 0.01	0.63 ± 0.03
1.05	1.14−1.18	0.40−0.45	0.53 ± 0.01	0.54 ± 0.00	0.49 ± 0.01

[a] The equivalent sphere radius R_{eq} of a rod (Pt−Au−PPy) or a rod−sphere doublet is the radius of a sphere which has the same drag coefficient. The lower (higher) values correspond to rods of 2.5 (3.2) μm length, for cargo of the indicated radii. (The variation of length of the rods arises due to the polydispersity of PPy segments. The lengths of the Pt and Au segments were approximately 1.2 μm each, while the length of the PPy ranged from 0.1 to 0.8 μm).

Debye layer around the motor. The corresponding reaction force of the ions on the motor is the primary motive force. The motor generates force throughout the Debye layer, which is comparable in thickness to the motor radius. Because of the thick Debye layer, it is not appropriate to analyze the situation in terms of slip velocity, as done by Golestanian et al. in recent interesting work on design of phoretic motors.[16] The force on the ions is rapidly transferred to the fluid, from whence some of it returns to the motor via viscous back-reaction. Using the generalized Lorentz reciprocal relation we can write

$$\gamma \vec{U} = \vec{F}_{direct} + \int \vec{v} \cdot \vec{f}\, dx \quad (1)$$

for the velocity $\vec{U}$ of the doublet in translational motion along its symmetry axis, where γ is the drag coefficient, $\vec{F}_{direct}$ is the motive force, and the integral is the viscous back-reaction where $\vec{f}$ is the force density on the fluid resulting from the electric field set up by the motor's electrochemical activity and $\vec{v}$ is the fluid velocity which would be induced if the rod moved at unit speed in the absence of electrochemical activity.[17]

Separation of the cargo from the catalytic part of the motor suggests that the cargo should not have a large effect on motor function, so we will assume that the magnitude of $\vec{F}_{direct}$ is independent of the cargo size. The viscous back-reaction is difficult to estimate without detailed knowledge of the fields set up by electrochemical activity. If the back-reaction was independent of cargo size, the speed of a doublet would be inversely proportional to the drag coefficient γ. Naively, the viscous back-reaction is expected to be both negative (impeding motion) and increasing with the cargo size, so that the assumption of cargo independence should lead to an overestimate of the speed of large doublets relative to small doublets. Interestingly, the experiments reveal a correction in the opposite direction.

Since there are no closed-form expressions or useful approximations for the Stokes drag on a body shaped like our rod−sphere doublet, we compute γ via the completed double-layer boundary-integral equation method (CDL-BIEM).[18] This technique uses an indirect representation of the flow around a moving particle via point-force sources, with a singularity inside the particle and a force-dipole density on the surface. The latter is the principal unknown and is found through numerical solution of an integral equation on the particle surface. This method is well-suited to calculating particle mobility because the fluid bulk does not have to be treated explicitly. We express the drag coefficient in terms of the radius of a sphere with the same hydrodynamic drag as the doublet: R_{eq}, so that a doublet moving at speed U incurs a hydrodynamic drag $6\pi\eta R_{eq}U$. From γ we compute the ratio of doublet speed to rod speed ($U_{doublet}/U_{rod}$) for different cargo sizes and compare them to the experimental ratios (Table 3). The range of equivalent radii corresponds to the experimental range in lengths of PPy segments: the smallest corresponds to 2.5 μm long rods (a 2.4 μm motor plus a 0.1 μm PPy segment) and the largest to 3.2 μm long rods (0.8 μm PPy segment). If the viscous back-reaction were independent of cargo size, we would expect the speeds of doublets to be inversely proportional to the equivalent radius. The ratios of cargo-loaded speed to unloaded speed calculated under this assumption are shown in Table 3. Corresponding experimental ratios are shown in the last three columns. Although the origin of the anomalously high mobility for the doublets with the largest-radius cargo is unknown, it does bode well for future applications.

In conclusion, we have demonstrated the feasibility of using the Pt−Au−PPy/H_2O_2 motor system for transport of microsphere cargo. The motor function is not disrupted due to the presence of passive cargo although a decrease in speed was observed. Magnetic Ni segments incorporated into the rods quench the rotational diffusion (and biased rotation) in the presence of an external magnetic field, making such doublets ideal for cargo pick-up and delivery. Chemotaxis of Pt−Au rods was also used to transport cargo to a region of high H_2O_2 concentration. Many interesting applications can be envisioned for such cargo-bearing motors in the mesoscale. Cargo can be concentrated at desired regions. This may find application in bottom-up assembly of colloids or for delivery of materials at a specific location whereupon further binding events may be triggered depending on cargo surface functionality. This would require the ability to pick up and drop off cargo. The concentration of colloids against natural tendency to diffuse is made possible by coupling with the motor−fuel interaction that lowers the overall free energy of the system.

Acknowledgment. This work was supported by NSF-NIRT CTS-0506967.

Supporting Information Available: (1) Video clips of Pt−Au−PPy motor−1.05 μm radius cargo doublet, (2) time-dependent diffusion coefficients of rod and rod cargo doublets, (3) Pt−Ni−Au−Ni−Au−PPy motor−cargo doublets (0.6 μm radius cargo) in the absence and presence of

external magnetic field, and (4) chemotaxis of Pt−Au−PPy 0.6 μm radius cargo doublets toward gel containing 30% H_2O_2. This material is available free of charge via the Internet at http://pubs.acs.org.

References

(1) *Interfacial Electrokinetics and Electrophoresis*; Delgado, Á. V., Ed.; Marcel Dekker, Inc.: New York, 2002.

(2) (a) Watarai, H.; Suwa, M.; Iiguni, Y. *Anal. Bioanal. Chem.* **2004**, *378*, 1693–1699. (b) Vickrey, T. M.; Garcia-Ramirez, J. A. *Sep. Sci. Technol.* **1980**, *15*, 1297–1304.

(3) (a) Block, S. M. *Nature* **1992**, *360*, 493–495. (b) Ashkin, A. *IEEE J. Sel. Top. Quantum Electron.* **2000**, *6*, 841–856. (c) Agarwal, R.; Ladavac, K.; Roichman, V.; Yu, G.; Lieber, C. M.; Grier, D. G. *Opt. Express* **2005**, *13*, 8906–8912.

(4) (a) Bohm, K. J.; Stracke, R.; Muhlig, P.; Unger, E. *Nanotechnology* **2001**, *12*, 238–244. (b) Soong, R. K.; Bachand, G. D.; Neves, H. P.; Olkhovets, A. G.; Craighead, H. G.; Montemagno, C. D. *Science* **2000**, *290*, 1555–1558. (c) Weibel, D. B.; Garstecki, P.; Ryan, D.; DiLuzio, W. R.; Mayer, M.; Seto, J. E.; Whitesides, G. M. *Proc. Natl. Acad. Sci. U.S.A.* **2005**, *102*, 11963–11967.

(5) Purcell, E. M. *Am. J. Phys.* **1976**, *45*, 3–11.

(6) Paxton, W. F.; Sundararajan, S; Mallouk, T. E.; Sen, A. *Angew. Chem., Int. Ed.* **2006**, *45*, 5420–5429.

(7) Paxton, W. F.; Sen, A.; Mallouk, T. E. *Chem. Eur. J.* **2005**, *11*, 6462–6470.

(8) Paxton, W. F.; Baker, P. T.; Kline, T. R.; Wang, Y.; Mallouk, T. E.; Sen, A. *J. Am. Chem. Soc.* **2006**, *128*, 14881–14888.

(9) Wang, Y.; Hernandez, R. M., Jr.; Bingham, J. M.; Kline, T. R.; Sen, A.; Mallouk, T. E. *Langmuir* **2006**, *22*, 10451–10456.

(10) Kline, T. R.; Paxton, W. F.; Wang, Y.; Velegol, D.; Mallouk, T. E.; Sen, A. *J. Am. Chem. Soc.* **2005**, *127*, 17150–17151.

(11) Paxton, W. F.; Kistler, K. C.; Olmeda, C. C.; Sen, A.; St. Angelo, S. K.; Cao, Y.; Mallouk, T. E.; Lammert, P. E.; Crespi, V. H *J. Am. Chem. Soc.* **2004**, *126*, 13424–13431.

(12) Kline, T. R.; Paxton, W. F.; Mallouk, T. E.; Sen, A. *Angew. Chem., Int. Ed.* **2005**, *44*, 744–746.

(13) Hernandez, R. M.; Richter, L.; Semancik, S.; Stranick, S.; Mallouk, T. E. *Chem. Mater.* **2004**, *16*, 3431–3438.

(14) Caswell, K. K.; Wilson, J. N.; Bunz, U. H. F.; Murphy, C. J. *J. Am. Chem. Soc.* **2003**, *125*, 13914–13915.

(15) Hong, Y.; Blackman, N. M. K.; Kopp, N. D.; Sen, A.; Velegol, D *Phys. Rev. Lett.* **2007**, *99*, 178103−1178103−4.

(16) Golestanian, R.; Liverpool, T. B.; Ajdari, A. *New J. Phys.* **2007**, *9*, 2630–2637.

(17) (a) Kim, S.; Karrila, S. J. *Microhydrodynamics: Principles and Selected Applications*; Dover Publications: Mineola, NY, 2006. (b) Teubner, M. *J. Chem. Phys.* **1982**, *76*, 5564–5573.

(18) (a) Power, H.; Miranda, G. *SIAM J. Appl. Math.* **1987**, *47*, 689–698. (b) Power, H.; Wrobel, L. C. *Boundary Integral methods in fluid mechanics*; Computational Mechanics Publications: Southampton, 1995. (c) Karrila, S. J.; Kim, S. *Chem. Eng. Commun.* **1989**, *82*, 123–161.

NL072275J